Charge-exchange processes in collisions of H^+, H_2^+, H_3^+, He^+, and He_2^+ ions with CO and CO_2 molecules at energies below 1000 eV

S. Werbowy[*] and B. Pranszke[†]

Institute of Experimental Physics, University of Gdansk, ul. Wita Stwosza 57, PL-80-952 Gdansk, Poland

(Received 25 September 2015; revised manuscript received 28 January 2016; published 26 February 2016)

Absolute measurements of charge-exchange cross sections of H^+, H_2^+, H_3^+, He^+, and He_2^+ ions in CO and CO_2 have been made for energies below 1000 eV, an equivalent of the energy of ionized particles at typical solar-wind conditions. An attenuation method for the case of complex ions of a molecule, taking into account the influence on the ion beam composition of the processes of disintegration of the primary ions into secondary ones with different charge-exchange cross sections, is described. Also the secondary effects, like three-body collisions and re-ionization processes that could emerge at higher pressures of the gas layer, are discussed. Dependence of the cross sections on the number of atomic centers in the projectile have been explained on the basis of the energy defect of the reactions and asymmetric near-resonant charge-exchange process between the ion and target molecule including the Doppler broadening in the interaction of the monoenergetic ion beam and target molecules having an isotropic Maxwellian velocity distribution corresponding to room temperature. Using the semiempirical approach based on the parametrized numerical coupled-channel two-state calculations, we have extrapolated the cross sections to a broader range of velocities.

I. INTRODUCTION

Ion-molecule collisions are among the most common processes that are observed in various environments like the upper layers of the planet's atmosphere, interstellar matter near a star emitting a stream of ionized particles, as well as in the gas coma formed around comets approaching the Sun. The major source of ions in space are the stars. Main components of the stellar wind are protons H^+ (approximately 95%) and He^{2+} (approximately 4%). However, other singly charged ions are observed, mostly He^+. The continuous stream of ionized particles present in the stellar wind have velocities ranging from 2000 km/s from hot massive stars to velocities of about 20 km/s from cooler stars (for protons, this would correspond to energies up to 20 keV). The Sun is a medium-sized star with solar-wind velocities ranging from 200 up to 700 km/s, equivalent to a 0.2–2.6 keV energy range for protons.

CO is the most abundant molecule after H_2 in the interstellar matter [1], which makes CO the tracer of the H_2. From among the many cometary volatiles, CO and CO_2 are the most abundant components after water [2,3]. Moreover, the atmosphere of two neighboring planets with Earth, i.e., Venus and Mars, are composed mainly of CO_2. CO_2 is very difficult to detect by ground devices due to strong absorption by atmospheric CO_2, therefore, it may be more abundant in outer space than present estimates indicate.

The ions passing through the gas media could be neutralized through a charge-exchange process or disintegrated in case of molecular ions. At the same time, the target molecule may ionize or dissociate into smaller fragments. The collisions of H^+ and He^+ ions, because of their importance, are very well reported in the literature for a wide energy range. For higher energies, the cross sections for ionization of CO and CO_2 by 5–4000 keV protons and for electron capture by 5–150 keV protons have been a subject of studies reported in [4]. Cross sections for ionization of CO and CO_2 and for electron capture by He^+ ions in the 10–2000 keV and 5–350 keV energy range, respectively, have been reported in [5] and in the energy range 0.3–1.8 MeV in [6]. For both ions, at energies close to 45 keV, the electron capture cross sections have the same value as the ionization cross section. For higher energies, collisionally induced ionization of the target molecule (without changing the ion charge) is more important than the electron capture process. On the other hand, at lower energies, the electron capture process is dominating over the ionization of the target molecule, and ions are neutralized more frequently. For smaller energies, there are several reports available, e.g., for H^+ ions: in the 0.2–4 keV range [7], 1–5 keV [8], and 0.3–7.5 keV [9], respectively, for the He^+ ions: 0.2–4 keV [10] and 1–3 keV [11].

The collisions of main components of the solar wind with the two most common molecules in outer space, i.e., CO and CO_2, are very important for astrophysics and for studies of comets. However, we found that studies of the charge-exchange cross sections in CO and CO_2 for molecular ions, e.g., H_2^+, H_3^+, and He_2^+, were devoted much less attention. These ions are much less common, nevertheless they have been observed in various environments in outer space. The possibility of forming H_2^+ pickup ions in the stellar wind flow as a result of outgassing of interplanetary dust by primary solar wind ions, have been theoretically analyzed in [12]. The role of H^+ and H_3^+ ions in interstellar chemistry has been studied from the viewpoint of the degradation of the interstellar molecules [13].

The helium dimer cation He_2^+ can exist only in the ground state and also, because its first excited state is repulsive with only a very small van der Waals minimum at 5.3 Å, was not yet observed in interstellar matter. However, it can be formed in laboratory conditions in a helium electrical discharge and, because of its chemical properties, we have also placed our interest in investigating this molecule.

---
[*]s.werbowy@ug.edu.pl
[†]Present address: Faculty of Marine Engineering, Gdynia Maritime University, ul. Morska 81-87, 81-225 Gdynia, Poland.
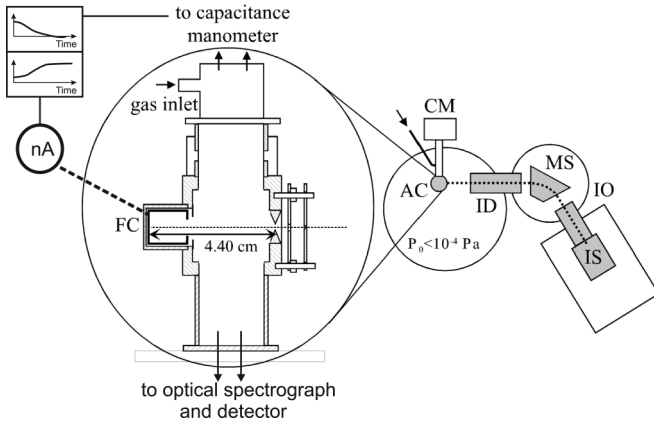
FIG. 1. Ion beam attenuation experimental setup. IS ion source, IO ion extraction and ion optic devices, MS mass selector, ID ion deceleration, AC attenuation chamber, CM capacitance manometer, and FC Faraday cup.

Charge exchange for 40–1500 eV H_2^+ ions in CO_2 has been reported in [14], and was reinvestigated for the 30–500 eV energy range in [15]. In the case of He_2^+ ions, only thermal energy rate constants with CO have been determined in pulsed discharge in the He/CO gas mixture [16].

Collisions of the H^+ and H_3^+ ions with CO_2 have been reported recently in [17], for the H_2^+ ions in [18] and for the He^+ in [19]. However, in these works only UV-Vis luminescence spectra and relative photon yield were reported with very rough estimates on the order of magnitude of absolute luminescence cross sections. Absolute luminescence cross sections for the H_n^++CO ($n = 1,2,3$) collision systems have been studied in [20].

In the present paper we have investigated the charge-exchange processes between hydrogen ions H^+, H_2^+, and H_3^+ and helium ions He^+ and He_2^+ with carbon monoxide and carbon dioxide at ion velocities typical for the solar wind, i.e., below 1000 eV. For this purpose we have used the attenuation method, based on the measurement of the attenuation of the ions passing the gas target of known concentration and thickness of the layer.

The accurate experimental data on charge-exchange cross sections between ions and molecules are essential for a clearer analysis of observations. First, the measurements of collisions of H^+ and He^+ ions with CO and CO_2 serve to check the accuracy of the method used, since the data for these elementary collisions are well known in the literature. Additionally, for the He^++CO_2 system, there is a large discrepancy between values of [9] and two times smaller values of [10]. Based on the cross section measurements [9], we discussed inconsistencies in observations of the *Giotto* spacecraft during a close encounter with comet Halley in 1986. Later values of [10] could cast doubts on these conclusions, this has motivated us to repeat these measurements to settle between these two results.

In the next step we measured the charge-exchange cross sections for hydrogen and helium molecular ions. We also discuss the influence of the secondary effects, like three-body collisions at high pressures, the re-ionization processes, or disintegration of molecular ions.

II. EXPERIMENT

In the experiment we used the apparatus described in detail in, e.g., [21] (and references cited therein). It is an ion beam-gas
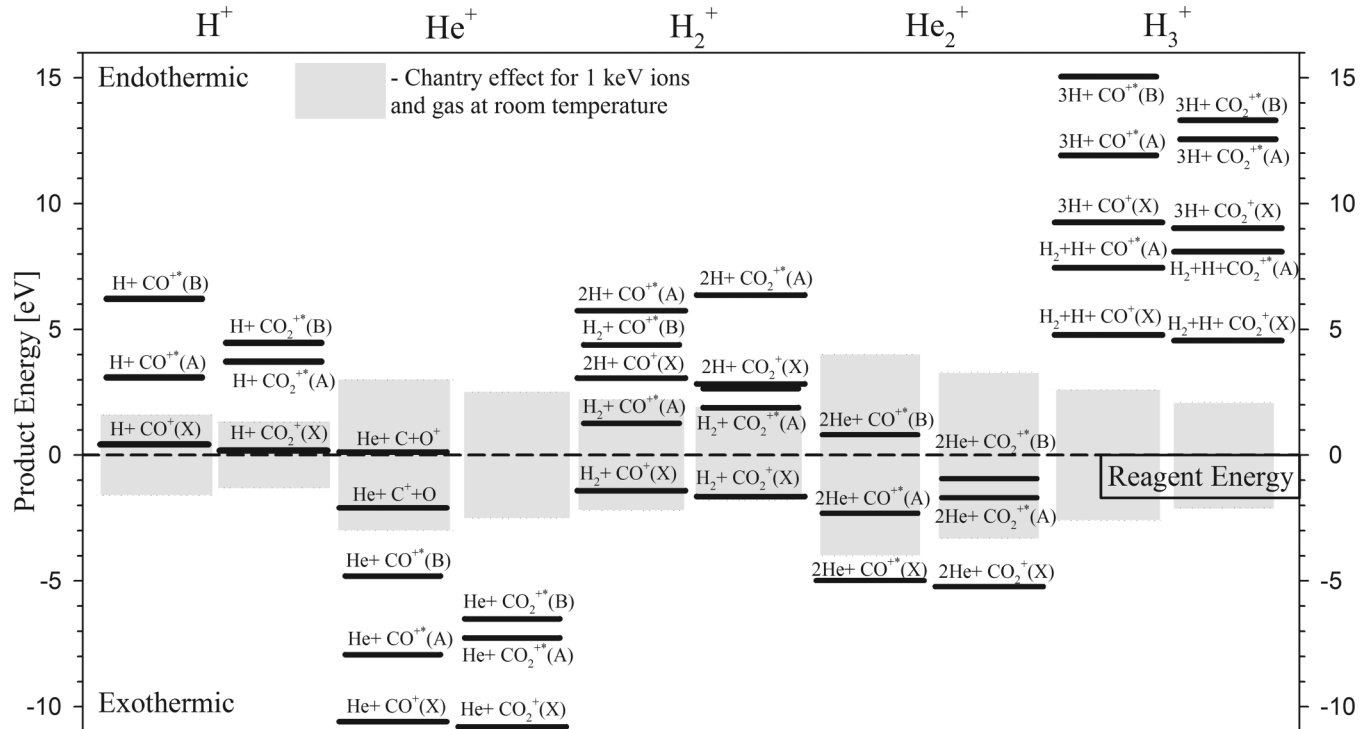

FIG. 2. Asymptotic energies of the charge transfer reaction products calculated with the help of the data presented in Table I. Zero of the energy scale is for reagent ground state. The shaded gray areas indicate the Doppler full width at half-maximum of the Chantry effect [41].

arranged system with a hot-cathode ion source, operating on He or H_2 gas at a pressure of about 200–400 Pa. The ions are extracted from the source and accelerated by a 1000 V potential. The beam is formed by means of ion optics lenses, and passes a magnet which separates the paths of ions with different mass or charge ratios. The ions of the desired species travel into the interaction chamber, which is located approximately 1 m from the ion source. Before the collision cell, the ions were decelerated to the desired laboratory energy. Originally this apparatus was designed to study the UV-Vis luminescence produced in the charge transfer reactions of sub-keV ions with gases [22,23] or chemiluminescent insertion reactions between neutral atoms and gases [24]. For the purpose of the present studies we have made a modification of the reaction chamber to adapt it to the attenuation measurements of ions, a schematic of the apparatus is shown in Fig. 1. The ions enter the charge-exchange chamber through a 1 mm entrance slit, and after passing 4.4 cm path through the gas, the remaining ions are collected in a 1.5 cm deep Faraday cup. The collision chamber was filled with CO or CO_2 gas at pressures below 1.3 Pa (10 mTorr) as measured with a Barocel capacitance manometer connected with the charge-exchange chamber as close as possible through a large conductance 1 in. pipe ensuring that there is a small pressure difference between the two points. The background pressure was kept below 10^{-4} Pa.

The influence of recoil ions that are products of the charge transfer dissociation channel on the recorded ion current is rather insignificant, the C^+ and O^+ recoil ions ejected at a 70° angle from 20 keV H^+ colliding with CO and CO_2 have energy of only a few percent of the energy of the incoming ion [25]. Main charge transfer products CO^+ and CO_2^+ are expected to have energies even smaller, by a factor of 2. Although, at

TABLE I. Asymptotic limit energies of the reaction components.

Reaction component	Ionization energy (eV)	Dissociation energy (eV)
H	13.598[a]	–
He	24.587[a]	–
H_2	15.42593[b]	4.477[c]
CO	14.014[b]	11.11[c]
CO_2	13.777[b]	5.45[c] ($CO_2 \rightarrow CO + O$)
He_2	22.223[d]	1.36[e]

The effective recombination energy
$(He_2^+ + e^-) \rightarrow$ 2He +(18.3–20.3) eV[f]
with maximum occurring at about 19 eV[f]

Total product kinetic energies in
the dissociative recombination

H_3	$(H_3^+ + e^-) \rightarrow \begin{cases} 3H(1s^2 S) + 4.76 eV^g \\ H_2(X\,^1\Sigma) + H(1s^2 S) + 9.23 eV^g \end{cases}$

[a]Reference [29].
[b]Reference [30].
[c]Reference [32] and references therein.
[d]Reference [31].
[e]Reference [33].
[f]Reference [34].
[g]Reference [35].

angle of 70°, the CO^+ and CO_2^+ recoil ions were not even detected [25]. This means that under present conditions the energies of the recoil ions would be very small (<20 eV). An effective path length for a few hundred eV recoil ions from collisions at gas pressures 0.3–0.6 mTorr given in [25] was approximately 5 cm. Assuming dependency of the mean path length to be inversely proportional to the pressure, this allows us to estimate its value for higher pressures (up to 10 mTorr) to be much less then 1 cm. At low gas concentrations the mean free path could be larger than the sizes of the Faraday cup, however the number of recoil ions would then be much smaller compared to the present in the beam projectile ions from which the recorded current would dominate. On the other hand, at high pressures the number of recoil ions increases, but this competes with the smaller mean free path length for the recoil ions which reduces the chances for them to reach the Faraday cup. Moreover, recoil ions produced in the main part of the chamber, which is 2/3 of the total thickness of the gas layer, due to aperture have minor chances to reach the surface of the Faraday cup.

The measuring procedure was as follows. First, the chamber was filled with the gas at approximately 10 mTorr pressure. When the pressure and ion current passing through the gas stabilized, we closed the feeding valve, allowing the pressure to decrease as the gas escapes to the vacuum. This initialized the procedure of simultaneous measurement of the pressure decrease inside the chamber and the change of the ion current. All parameters were recorded at the same time with the sampling ratio of 100/s. A single measurement lasts approximately 10 s, until the pressure has decreased to 0 mTorr. Typical H^+, H_2^+, and H_3^+ ion currents were approximately 13 nA/mm², and for the He^+ and He_2^+ ions ~50 nA/mm² and less than 1 nA/mm², respectively. The ion current fluctuations were approximately 10% of the mean value. We intentionally have used the anode-to-cathode voltage on the 50 V level to reduce the formation of electronically excited He^+ ions.

III. ATTENUATION OF THE H⁺ AND He⁺ IONS

The charge transfer collision processes involving protons are slightly endothermic ($\approx$0.3 eV), while collisions of the He^+ ions with CO and CO_2 are very exothermic reactions (with energy defect $\approx$10 eV). Figure 2 presents the energies of the reaction products calculated with the help of the data given in Table I.

In order to measure the charge-exchange absolute cross sections we have used the attenuation method. This has been partly dictated by low values for some of the ion currents. For the charge-exchange (CE) collisions involving the simple H^+ and He^+ ions with CO and CO_2 molecules:

$$H^+ + G \rightarrow H^* + G^{+*} \quad (CE), \qquad (1)$$
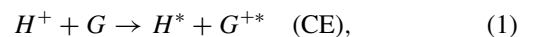
the method can directly give the charge-exchange cross sections. Here the asterisk indicates that the products could be either ground or excited states. When a beam of singly charged ions passes the attenuating media G, where they can be neutralized through interaction with the gas, we can give the following differential equations describing the $H^+ \rightarrow H$ process:

$$\frac{d[H^+]}{dN} = -\sigma_{10}L[H^+], \quad \frac{d[H]}{dN} = \sigma_{10}L[H^+], \quad (2)$$

$$[H^+](0) = I_0, \quad (3)$$

where $[H^+]$ and $[H]$ are the number of ions and neutral atoms in the beam, N is the gas concentration, σ_{10} is the cross section for the charge-exchange process, and L is the gas layer thickness. Here we have assumed the conditions where only two-body collisions take place, this is ensured by the relatively low gas pressures. The solutions for this equations with the boundary conditions are

$$[H^+](N) = I_0 e^{-\sigma_{10}LN}, \quad (4)$$

$$[H](N) = I_0(1 - e^{-\sigma_{10}LN}). \quad (5)$$

The ion current recorded in the Faraday cup depends exponentially on the gas concentration and thickness of the layer.

The attenuation plot of H^+ and He^+ ions in the CO and CO_2 at an ion energy of 1000 eV and pressures below 6 mTorr are presented on the semi-log scale in Fig. 3. The origin of the observed scatter of the experimental points are random current fluctuations of the ion beam in the Colutron-type hot-cathode ion source. Since the current is recorded at a high speed of 100 points per second, it is possible to observe them as a symmetrical scatter of points around the best fit exponential line. In addition, in some parts of the attenuation plots nonsymmetrical deviation of the experimental points from the best fit line can be observed. It is a consequence of the unexpected temporary deviation of the ion beam path from the position of the small entrance slit. This is due to static charges collected on the electrostatic lenses or other components of the ion optics.

Figure 4 presents a compilation of experimental and theoretical absolute charge-exchange cross sections for H^+ and He^+ with CO and CO_2 at the ion velocities in the range 100–5300 km/s and 80–3500 km/s for H^+ and He^+ ions, respectively. It should be noted that the present data (filled black circles) are obtained directly from the measurements of the gas concentration and are not corrected or calibrated to any other data. In addition to the experimental data, we have imposed also a cross section calculated by using the Oslon formulas [36] (see Appendix A) with parameter values given in Table II. The gray shaded areas indicate the variation of the Olson formula calculations when assuming $\Delta\lambda = \pm 5\%$ and $\Delta E, \Delta R_c = \pm 10\%$ of the values given in Table II.

Presented results are mean values and mean standard deviations out of several independent measurements. Additionally, the experimental errors were increased by 10% of the charge-exchange values. This includes the fact that in the determination of σ_{10} we have assumed the thickness of the gas layer L equal to the distance between the entrance slit and the surface of the Faraday cup, 4.4 cm. However, the pressure or concentration of the gas is not homogeneous along the entire L path. The gas is escaping into the background pressure area, thus in the vicinity of the entrance slit the concentration is smaller. We roughly estimate the relative uncertainty of the thickness of the layer $\Delta L/L$ on the $\pm 10\%$ level.
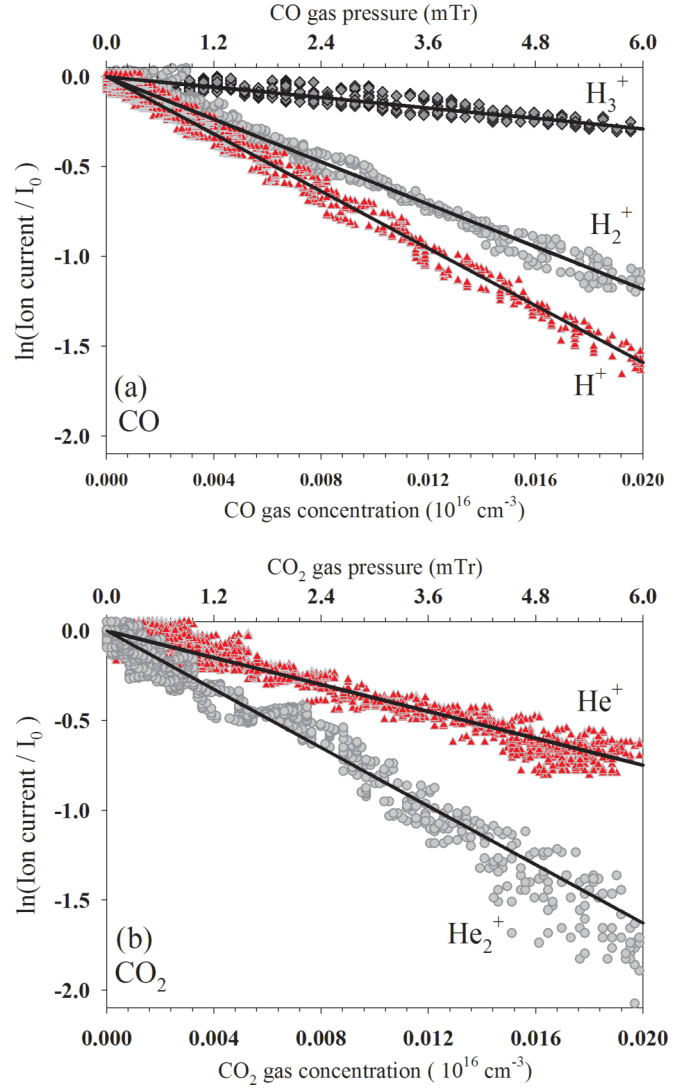

FIG. 3. (a) Attenuation plots in CO of H^+, H_2^+, and H_3^+ ions and (b) attenuation plots in CO_2 of He^+ and He_2^+ ions at the energy of 1 keV in the laboratory frame. I_0 is the ion current without gas target ($N = 0$).

As can be observed from Fig. 4, in case of H^+ ions our data are in good agreement with other measurements. For He^+ ions our results are in agreement with some of the experimental data, but there are significant discrepancies between different authors.

TABLE II. Values of the parameters in the model of Olson [36], adopted in the calculations presented in Figs. 4 and 6.

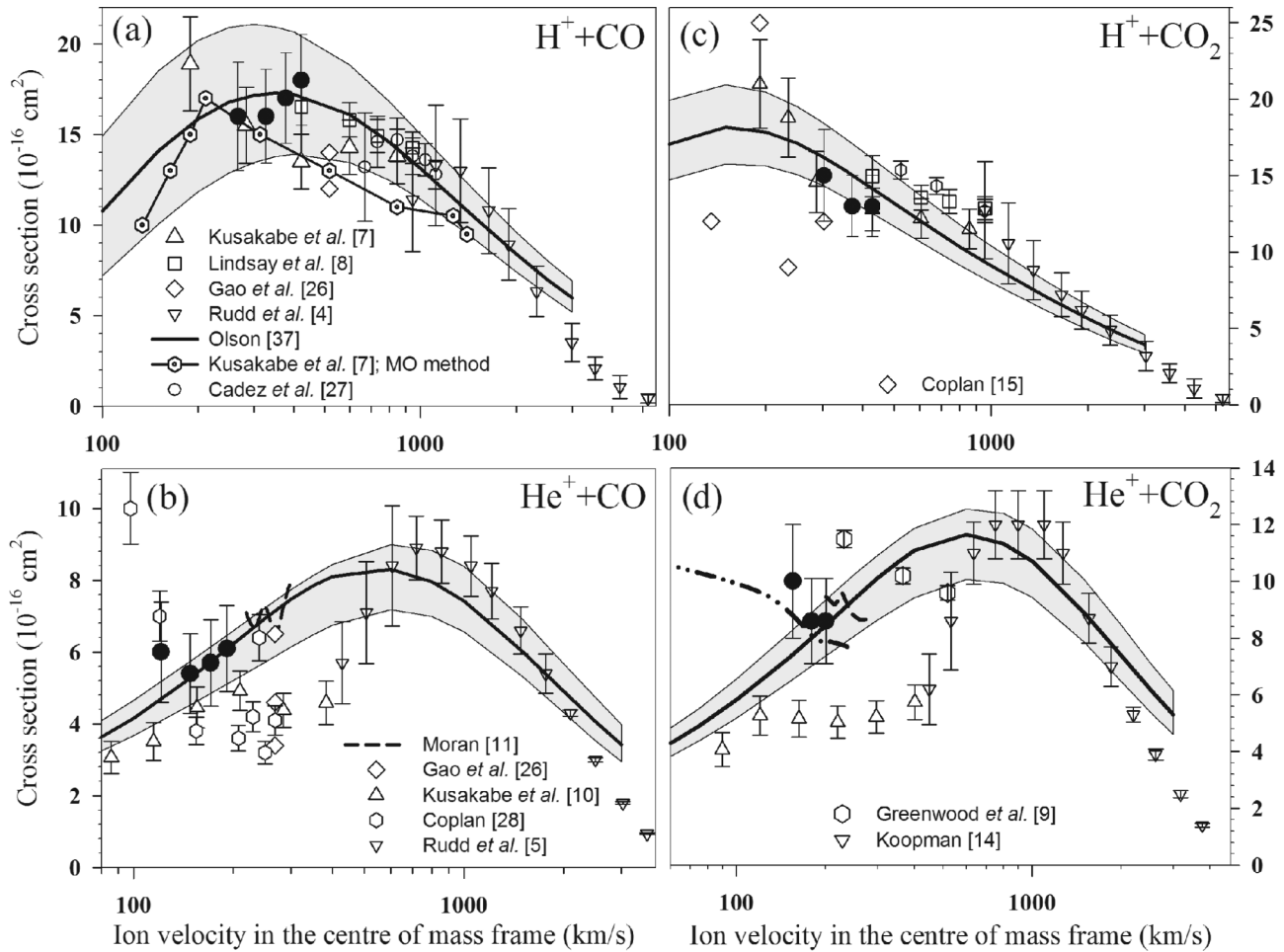|	CO			CO_2		
	λ (Å^{-1})	ΔE (eV)	R_c (Å)	λ (Å^{-1})	ΔE (eV)	R_c (Å)
H^+	0.73	-0.416	3.0	0.84	-0.18	2.5
H_2^+	0.65	1.41	3.2	0.65	1.65	3.0
H_3^+	0.80	-4.78	3.0	0.75	-4.55	2.5
He^+	0.88	10.6	1.6	0.76	10.8	1.7
He_2^+	0.40	8.21	2.6	0.45	8.45	2.4

FIG. 4. Charge-transfer cross sections for H^+ and He^+ ions in the collisions with CO (boxes a and b) and CO_2 (boxes c and d) molecules. Filled black symbols are the present data.

For higher pressures one could expect the secondary effects due to the three-body collisions or the two-step neutralization–re-ionization process. Their influence is discussed in detail in Appendix B. The straight lines in the attenuation plots presented in Fig. 3 indicate that the present measurements fulfill a two-body condition. For our conditions, the pressures were too small to clearly observe the secondary effects, which are expected to be much smaller than charge-exchange processes σ_{10}. Figure 5 presents the influence of the K parameter from Eq. (B3) on the nonlinear behaviors of the attenuation plots. The nonlinear effects could be observed at pressures higher than 6 mTorr. Figure 5 presents the attenuation curve of the He^+ ions on CO for pressures up to 44 mTorr. From comparison with the calculated attenuation curves we see that nonlinear effects are minor even at such high pressures, and the K coefficient is smaller than 6×10^{-32} cm^5. This concludes that target gas pressures used in the present measurements, i.e., below 6 mTorr, comply with the condition $KN/2 \ll \sigma_{10}$, allowing for the neglecting of nonlinear effects.

From the analysis of results from [4,5], we have concluded that for small energies used in the present studies, the electron loss cross sections σ_{01} are expected to be much smaller than charge-exchange cross sections σ_{10}, thus re-ionization influence on the observed ion current is negligible. For instance, the σ_{01} for 1 keV H atoms in CO and CO_2 are 0.83 and 0.95 Å^2, respectively [8]. For the CO molecule this is 20 times and for the CO_2 16 times less than electron capture cross section σ_{10} for the H^+. On the basis of the above we conclude that at present conditions the secondary effects are less important, this will result in the single exponent attenuation plots that have been observed.

At this stage we conclude that our method and conditions used are suitable to give reliable values of the charge-exchange cross sections, and it is possible to measure the cross sections for other ions, i.e., H_2^+, H_3^+, and He_2^+.

IV. ATTENUATION OF THE H_2^+, H_3^+ AND He_2^+ IONS

In contrast to the H^+ ions, electron capture collisions involving the H_2^+ ion are exothermic, but only for the case when the CO^+, CO_2^+ products are in the ground state. Collision processes involving He_2^+ ions are exothermic (≈ 7 eV) like in the case of the He^+ (see Fig. 2).

Electron capture reactions of the H_3^+ ions with CO and CO_2 could lead to the formation either of three hydrogen atoms or a pair of hydrogen atom with a hydrogen molecule, both channels are endothermic (see Fig. 2).
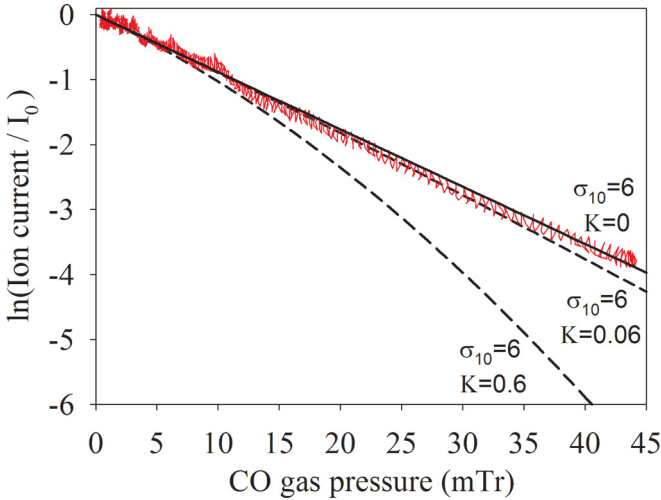
FIG. 5. The influence of the K parameter on the nonlinear attenuation plots. Values of σ_{10} are expressed in 10^{-16} cm^2 and K in 10^{-30} cm^5 units. The red line presents a recorded attenuation plot in CO at pressures up to 44 mTorr of He$^+$ ions at the energy of 1 keV in the laboratory frame.

Examples of the attenuation plots of the H$_2^+$ and H$_3^+$ ions in the CO and He$_2^+$ in the CO$_2$ at an ion energy of 1000 eV are presented on the semi-log scale in Fig. 3. For the He$_2^+$ ions we have very low currents, therefore it was difficult to establish stable conditions. Nevertheless, since the charge-exchange cross sections appear to be very high compared to other ions, it was possible to determine the slope from the attenuation plots.

Determined from the attenuation plots the absolute charge-exchange cross sections for the H$_2^+$, He$_2^+$, and H$_3^+$ with CO and CO$_2$ at energies below 1000 eV are presented in Fig. 6 (these energies correspond with the ion velocities of approximately 310, 250, and 150 km/s for H$_2^+$, H$_3^+$, and He$_2^+$ ions, respectively). For comparison we have presented available values obtained by other authors. The gray shaded areas indicate the uncertainty of the Olson formula calculations when assuming $\Delta\lambda = \pm 10\%$ and ΔE, $\Delta R_c = \pm 20\%$ of the values given in Table I.

However, in case of molecular ions we must keep in mind the possibility of influence of the secondary effects on the obtained results. For the H$_2^+$, H$_3^+$, and He$_2^+$ primary ions, in the attenuation method we should consider the possibility of the collisionally induced dissociation of the ion molecule into other ionic components somewhere in between the entrance slit and the Faraday cup. Formed in this way secondary ions are likely to have a different electron capture cross section and would affect the measured ion currents after passing the gas layer. We have found that at present conditions influence of the secondary ions is not so critical, we have discussed this in detail in Appendix C.

In conclusion, for the H$_2^+$, H$_3^+$, and He$_2^+$ primary ions, the values presented in Fig. 6 were determined in terms of the model assuming no disintegration of the projectile—a single exponential model. Therefore, it should be treated rather as the lower limit for the charge-exchange cross sections in CO and CO$_2$. From the analysis of solutions of Eqs. (C11)–(C13) presented in Fig. 7, we estimate that the final σ_{10} values for the H$_2^+$, H$_3^+$, and He$_2^+$ primary ions in CO and CO$_2$ could be higher,

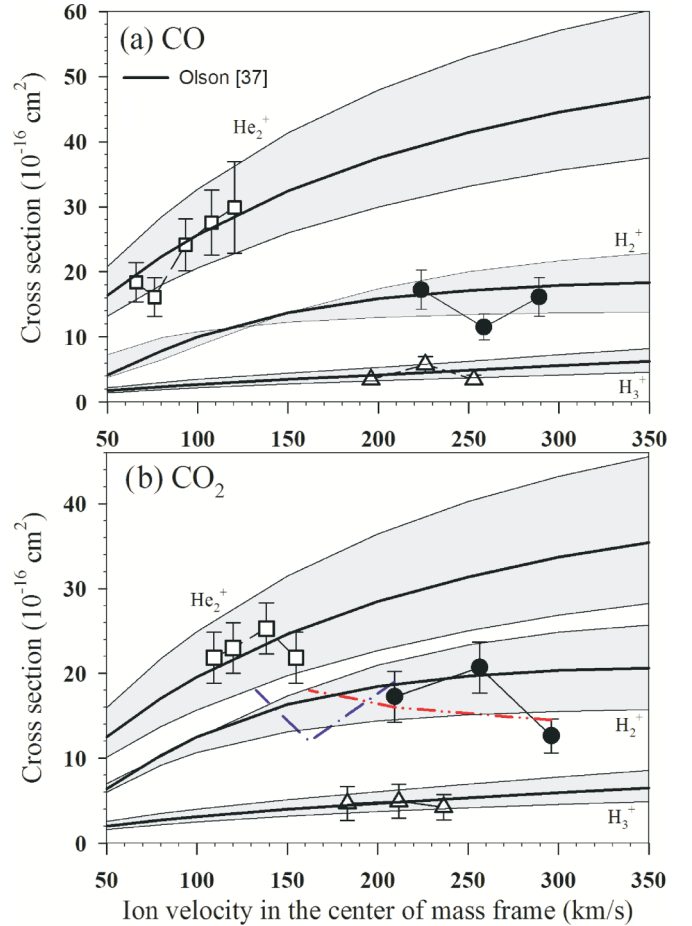FIG. 6. Charge-transfer cross sections for H$_2^+$, H$_3^+$, and He$_2^+$ ions in the collisions with CO (box a) and CO$_2$ (box b) molecules. The red dash-dot line is the data of [14] for the H$_2^+$ + CO$_2$, and the blue dash-dot-dot line presents the data of [15] for the H$_2^+$ + CO$_2$ system.

but no more than 15%–20%, depending on the unknown disintegration cross sections σ_d. The data presented in Fig. 6 include this and measured cross sections were increased by 15%.

V. CONCLUSIONS

In the present studies we have made measurements of all title collision systems on the same apparatus under similar experimental conditions in what we believe bears a small relative uncertainty. Other author measurements were usually performed for each system separately.

The data for the charge-exchange cross sections for H$^+$ and He$^+$ presented in Fig. 4 shows that our noncalibrated results are in agreement with most of the literature data.

In order to extrapolate the cross sections to a broader range of velocities, calculations in the semiempirical approach have been made with the formulas derived by Olson [36] (briefly described in Appendix A). The thick continuous lines in Figs. 4 and 6 present calculated cross sections with suggested parameter values given in Table I. The shaded gray area indicates the variations of calculated values when assuming uncertainties of parameters in the Olson theory. The λ parameters are in the range of (0.65–0.84) Å^{-1}

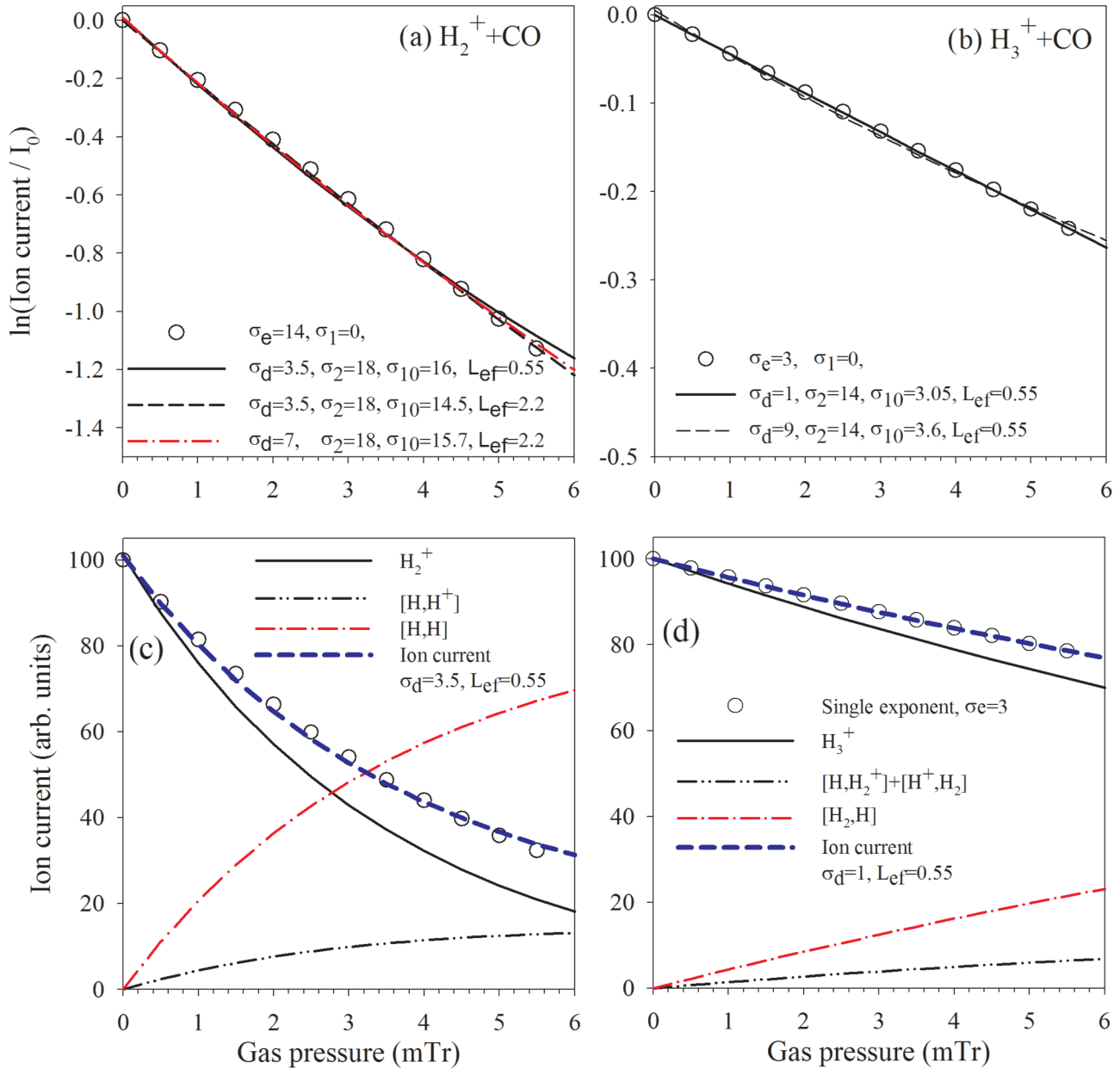FIG. 7. Solutions of the differential equations (C7)–(C9) including presence of disintegration of the H_2^+ (a) and (c) and H_3^+ (b) and (d) ions in CO, calculated for different values of the disintegration σ_d, charge exchange of the primary ions σ_{10} cross sections, and L_{ef} parameters. All σ values are expressed in 10^{-16} cm^2 units. Insets (a) and (b) present total ion current recorded at the Faraday cup in logarithmic scale. Insets (c) and (d) present the pressure dependency of specific beam components (C11)–(C13) at the position of the Faraday cup.

for the H_n^+ and He$^+$ ions. However, for the He$_2^+$ ion the coupling parameter λ is two times smaller, which means that coupling is stronger than in the case of the rest of the ions, making in this case the electron capture cross sections high.

In the case of He$^+$ ions there are significant differences between values of different authors. The difference between the present results and data of [9] or [10] for He$^+$ ions (see Fig. 4), which are significantly smaller, are difficult to explain and may be a result of undetected experimental systematic errors. In our studies we used the same method and gas pressure range used in [9]. In order to avoid contamination of the ion beam (for example by O^{4+}) ^{3}He isotopes have been used in [9]. Comparing the data, expressed as the velocity of the ion in

the center of mass frame instead of the ion kinetic energy, we notice that values of [9] and from the present studies are related to different velocities, thus they are hard to compare with each other. The data of [9] was collected for higher velocities and could be slightly higher. Nevertheless, both data are lying within the solutions of the extrapolated Olson model which predicts an increase of the cross sections with the velocity to reach a maximum at about 800 km/s (18 and 12 keV for CO and CO$_2$, respectively).

However, this does not explain the large discrepancies of data from [10]. From the description of the experimental details given in [10], especially a fragment "*gas pressure was monitored with a calibrated Pirani gauge,*" this suggests that the pressure, necessary to determine the gas concentration,

was measured with the gauge where the reading depends on the used gas. It could be that despite the good intentions of the investigators the gauge was not calibrated correctly. Unlike the Pirani gauges, the capacitance manometer operation is independent of the working gas. Possibly, the calibration was more accurate for the CO than CO_2 which has a reflection in smaller differences between values in the He^++CO collision system. The accurate pressure measurement is the most important issue in the measurements of the absolute cross sections.

Another source of the uncertainty could be the experimental method used by [10], i.e., direct measurement and the evaluation of the fractions of remaining He^+ ions and product neutral particles He in the beam detected on the position-sensitive detector consisting of a microchannel plate and a resistive anode as a function of the gas thickness. In their earlier papers they have made an assumption that "*It may be safe that relative detection efficiencies of the MCP-PSD were the same for both the singly charged ions and neutral particles as the front end of the MCP was grounded*" [7]. Smaller detection efficiency for neutral products (which after electron capture could be either in the ground as well excited metastable states [38]) with respect to ions would result directly in the smaller cross sections.

We believe that it is safe to conclude that recently published measurements of [10] do not undermine the data and conclusions stated by [9] on the observations made by the *Giotto* spacecraft during a close encounter with comet Halley in 1986.

From hydrogen ions, H_3^+ have the lowest electron capture cross section of all. Ion collisions with CO and CO_2 may have few common features with the H_2O or H_2 molecule. Collisions of hydrogen H^+, H_2^+, and H_3^+ ions with H_2O vapors for energies between 2 and 60 keV have been studied in [39]. The charge-exchange cross section ratio for ~2 keV H^+, H_2^+, and H_3^+ with H_2O are 100 : 50 : 10. The proportions of the average cross sections for CO and CO_2 at energies from present studies are 100 : 90 : 25 and 100 : 120 : 35, respectively. In the case of the H^+, H_2^+, and H_3^+ with H_2, extrapolating the data of cross section [40] to 2–3 keV, the proportions are 100 : 100 : 40. In all four molecules we notice a smaller electron capture cross section in the case of the H_3^+ ion.

The above findings may be related to the energy defect of the reactions and asymmetric near-resonant charge-exchange process between the ion and target molecule. It has been already established in a number of measurements that large cross sections are often associated with near-resonant charge-transfer processes. From Fig. 2 we see that the closer the energy of a given reaction product is to the reagent energy the higher the cross sections are. Additionally, one has to kept in mind that beside the spread of the ions energy, which in our experimental conditions is approximately 0.2 eV, a Doppler broadening in the interaction of the almost monoenergetic ion beam interacting with target molecules having an isotropic Maxwellian velocity distribution corresponding to a temperature should be considered. This effect has been described by Chantry [41] who gave the expression for the full Doppler widths at half-maximum when a beam of nominal center of mass energy interacts with gas at a given temperature. The shaded gray areas in Fig. 2 presents the Doppler widths at

nominal 1000 eV energies. The Doppler broadening arising from the thermal motions of the target gas makes that more final ro-vibrational product states are in resonance with the reagent energies.

The energies of the ground state products for the endothermic reaction H^+, H_2^++CO_n(X) are overlapping within the Doppler broadening with the energy of the reagents, which results in the observed high cross sections. For endothermic reactions with the H_3^+ ions, the product states are lying far away from the resonance, thus the cross sections are much smaller. This qualitatively explains the proportions between H^+, H_2^+, and H_3^+ cross section values. This interpretation applies also to the H_2O and H_2 molecules, where product energies present in Fig. 2 should be shifted up by 1.41 eV and down by 1.39 eV on the energy scale for H_2 and H_2O, respectively.

As follows from Fig. 2, the charge transfer reactions with He^+ ions are nonresonant, thus one should expect small cross sections. However, because they are exothermic processes, their cross sections are larger and are between near-resonant H^+ and H_2^+ ions and endothermic H_3^+ reactions. Additionally, from the spectroscopic studies a number of C, C^+, O, and O^+ lines have been identified in the UV-Vis luminescence spectra [38]. This indicates the presence of substantial collision-induced dissociation channels in the He^++CO for which the energy defect is shifted up on the energy scale towards the endothermic processes by 8.5 and 10.7 eV, considering the average appearance energies [42]: 22.5 eV for the CO $\rightarrow C^+$+O and 24.7 eV for the CO $\rightarrow$ C+O^+, respectively. The energy defect for the lowest ground states dissociated channel He(^1S)+C(^3P)+O^+(^4S) is close to the resonance. Although, from the energy balance the collision-induced dissociation channels are less exothermic, some of the products could be in near-resonance condition, therefore contributing to the total electron capture cross sections and to an attenuation of the He^+ ions from the beam.

In the case of the He_2^+ ions, from the spectroscopic studies [38] we have found that the luminescence cross sections for the He_2^++CO system leading to the excitation of the CO^{+*}(A), CO^{+*}(B) states are exceptionally high. For the CO^{+*}(A-X) and CO^{+*}(B-X) observed channels they sum up to about 20–30 $Å^2$ at collision energies above 500 eV and 12 $Å^2$ below that energy. The present data allow an estimate of the luminescence yield almost on the level of 100%. Opposite to the He^++CO luminescence spectra in the UV-Vis range, there was no evidence of the atomic emissions resulting from the collisionally induced dissociation channels for this ion. Even He lines have not been observed [38], which indicates that after the charge transfer process He_2 instantly dissociates into two He components in the ground or some metastable state (depending on whether the He_2 was in the very unstable ground state or as an electronically excited excimer molecule) that could not be detected in the luminescence measurements. The corresponding energy defects for the endothermic dissociation products would lie above the reagent energy including the Chantry widths. Based only on the energy defect we should expect that the cross sections for the He_2^+ ions with CO_n should be highest of all, since there are many ro-vibrational levels of the CO^{+*}(X,A,B) product states that overlap within the largest of all Doppler broadening of the target-gas-ion with the near-resonance reagent energies.

Additionally, in the case of He_2^+ ions another factor could play an important role in the exceptionally high cross sections. The He_2^+ ions are the biggest ones, the equilibrium bond distances are $r_e(He_2^+) = 1.08$ Å and $r_e(H_2^+) = 1.052$ Å. The equilibrium distance between two corners of the trihydrogen cation H_3^+ in triangular equilateral configuration is 0.86 Å [43], making it the smallest ion molecule studied here. In case of the H^+ and He^+ ions, from the point of view of a target molecule they are treated as the pointlike charges where energy defect (and more precisely the relationship between the potential energy surfaces) are important. When energy defect is small (a near-resonant charge transfer), it means that two potential energy surfaces of the reactant ($P^+ + T$) and product ($P + T^+$) states are close to each other and the radial coupling matrix element would be higher.

Present results support the conclusions given in [38] that the diatomic helium cation proved to be an excellent electron acceptor where charge-transfer collisions with CO can be a very efficient source of ionized target molecules in the excited electronic states. This finding could be very useful as the light source for spectroscopic characterization almost free of atomic lines.

The collisions of the H_2^+, He_2^+, and H_3^+ ions with various gases are found to be very interesting and should get more attention in both theoretical and experimental studies.

From the analysis of the attenuation plots with the help of the presented complex model including the influence of the secondary ions on the recorded current, we conclude that at present conditions, i.e., the range of the target gas pressures and the thickness of the layer, it is possible to obtain the reliable charge-exchange cross sections for molecular ions. Any deviation resulting from the presence of secondary ions is manifesting itself at pressures higher than 10 mTorr for the layer of 4.4 cm thickness.

The present data could have applications to the studies of the interaction of the solar wind particles with Venus [44] (pp. 873–940) and Mars [45] (pp. 454–456) atmospheres, which are composed mainly of CO_2. The weakness of the magnetic field of two planets makes them vulnerable to the direct influence of the ions on the atmosphere.

APPENDIX A: SEMIEMPIRICAL CHARGE TRANSFER CROSS SECTIONS

Olson [36] has performed numerical coupled-channel two-state calculations of the total electron capture cross sections for the case of near parallel potential curves of a reactant and product states. His calculations proved to be useful in estimations of the energy dependence of the charge-transfer inelastic total cross sections for several alkali ion–alkali

atom systems. Using a Smirnov method he found a formula applicable at high velocities:

$$\sigma_H(v) = \frac{1}{2}\pi R_0^2, \tag{A1}$$

R_0 can be found from the solution of

$$\frac{1}{v}\sqrt{\frac{2\pi R_0}{\lambda}}\frac{H_{12}(R_0)}{\hbar} = 0.28, \tag{A2}$$

$$H_{12}(R_0) = e^{-\lambda R_0}, \tag{A3}$$

where $H_{12}(R_0)$ is the coupling-matrix element that can be well approximated by the simple parametrized exponential function [36]. Calculating the cross section for high velocities and comparing it with the available experimental data we can find the value of the λ parameter.

At the threshold region and low velocities, Olson [36] has derived equations without using the Demkov formulas:

$$\sigma_L(v) = 4\pi R_c^2 \int_1^\infty \frac{e^{-\delta x}dx}{x^3(1 + e^{-\delta x})^2}, \tag{A4}$$

$$\delta = \frac{1}{v}\frac{\pi \Delta V(R_c)}{2\hbar\lambda}, \tag{A5}$$

where $\Delta V(R)$ is the difference between two potential curves defined as

$$\Delta V(R) = |V_r(R) - V_p(R)|$$
$$= \left|V_r(\infty) - V_p(\infty) - \frac{\alpha_r - \alpha_p}{2R^4}\right|, \tag{A6}$$

a long range ion-molecule interaction component contains the $\alpha_{r,p}$ dipole polarizability of the neutrals in the reagent and product states. In his calculations, Olson [36] has assumed that the charge transfer at low to moderate velocities is then found to be localized at the internuclear separation where $\Delta V(R_c) = 2H_{12}(R_c)$. This assumption can be used to find the values of missing $\Delta V(R_c)$ and R_c parameters necessary to calculate $\sigma_L(v)$.

The cross sections described by Eqs. (A1) and (A4) are applicable only at high and low velocities, respectively. In practice, the low-velocity cross sections join with the high-velocity cross sections only at one point after which each formulation is no longer applicable. This point would correspond to the moderate velocity region. In order to estimate the entire velocity range dependency of the cross section we have used both low (A1) and high (A4) velocity cross sections with weights proportional to the velocity:

$$\sigma(v) = e^{-v/v_m}\sigma_L(v) + (1 - e^{-v/v_m})\sigma_H(v). \tag{A7}$$

First, we are calculating the cross sections for high velocities and comparing it with the experimental data to find the dependence of the coupling-matrix element and the λ parameter. Next, using the spectroscopic constants in Eq. (A6) and by solving $\Delta V(R_c) = 2e^{-\lambda R_c}$ we are determining the region where the charge transfer occurs R_c and $\Delta V(R_c)$.

APPENDIX B: SECONDARY EFFECTS

For higher pressures one could expect the secondary effects due to the three-body collisions, the frequency of which

depends on the gas concentration, in this case the differential equations would be

$$\frac{d[H^+]}{dN} = -(\sigma_{10} + KN)L[H^+], \tag{B1}$$

$$\frac{d[H]}{dN} = (\sigma_{10} + KN)L[H^+], \tag{B2}$$

where K is the coefficient for the three-body collisions. The exact solutions are

$$[H^+](N) = I_0 e^{-(\sigma_{10} + KN/2)LN}, \tag{B3}$$

$$[H](N) = I_0 - [H^+](N). \tag{B4}$$

It is also possible that when the H^+ ion has been neutralized somewhere between the entrance slit and the surface of the Faraday cup, a fast neutral H atom produced in this way could re-ionize through the electron loss process somewhere during the rest of the way. The two-step neutralization–re-ionization process $H^+ \rightleftharpoons H$ with $\sigma_{10}(\rightharpoonup)$ and $\sigma_{01}(\leftharpoondown)$ cross sections could have influence on the recorded ion currents. The differential equations describing this process are

$$\frac{d[H^+]}{dN} = -\sigma_{10}L[H^+] + \sigma_{01}L_{ef}[H], \tag{B5}$$

$$\frac{d[H]}{dN} = \sigma_{10}L[H^+] - \sigma_{01}L_{ef}[H], \tag{B6}$$

$$[H^+](0) = I_0, \quad [H](0) = 0, \tag{B7}$$

where L_{ef} is the effective thickness of the layer where neutralized H atoms have to pass from the point of neutralization up to the Faraday cup. The exact solutions are

$$[H^+](N) = \frac{I_0}{1+U}\left(e^{-\sigma_{10}LN(1+U)} + U\right), \tag{B8}$$
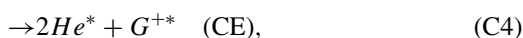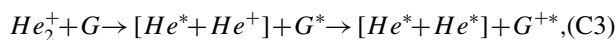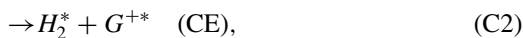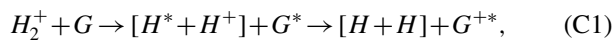
$$[H](N) = \frac{I_0}{1+U}\left(1 - e^{-\sigma_{10}LN(1+U)}\right), \tag{B9}$$

$$U = \frac{\sigma_{01}L_{ef}}{\sigma_{10}L}. \tag{B10}$$

When re-ionization (in other words a single-electron loss) cross sections are much smaller compared to the charge-changing cross sections ($\sigma_{01} \ll \sigma_{10}$) the above equations reduce themselves to Eqs. (4) and (5). The above formulas are applicable also for the He^+ ions.

APPENDIX C: DISSOCIATION OF THE MOLECULAR IONS

In the case of the H_2^+, H_3^+, and He_2^+ primary ions, in addition to the direct charge-exchange process in the attenuation method, we should consider the possibility of the disintegration of the ion into two components somewhere in between the entrance slit and the Faraday cup:

$$H_2^+ + G \rightarrow [H^* + H^+] + G^* \rightarrow [H + H] + G^{+*}, \tag{C1}$$

$$\rightarrow H_2^* + G^{+*} \quad (CE), \tag{C2}$$

$$He_2^+ + G \rightarrow [He^* + He^+] + G^* \rightarrow [He^* + He^*] + G^{+*}, \tag{C3}$$

$$\rightarrow 2He^* + G^{+*} \quad (CE), \tag{C4}$$

The recorded ion current will then be the sum of the primary molecular ions and the ionic products after disintegration. The secondary H^+ ionic products could have accidentally different charge-exchange cross sections than primaries H_2^+ and would be attenuated from the beam at a different frequency.

For the H_2^+ and He_2^+ primaries, in order to take into account the secondary ions, according to the scheme

$$H_2^+ \xrightarrow{\sigma_d} [H, H^+] \xrightarrow{\sigma_2} [H, H], \tag{C5}$$

$$H_2^+ \xrightarrow{\sigma_{10}} [H, H] \quad (CE), \tag{C6}$$
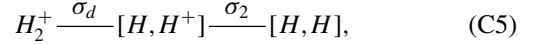
where σ_d is the disintegration cross section, σ_2 is the charge-exchange cross section for the secondary ion, and σ_{10} is the direct charge-exchange cross section, we need to solve the differential equations with the given boundary conditions:

$$\frac{d[H_2^+]}{dN} = -(\sigma_d + \sigma_{10})L[H_2^+], \tag{C7}$$

$$\frac{d[H, H^+]}{dN} = \sigma_d L[H_2^+] - \sigma_2 L_{ef}[H, H^+], \tag{C8}$$

$$\frac{d[H, H]}{dN} = \sigma_2 L_{ef}[H, H^+] + \sigma_{10}L[H_2^+], \tag{C9}$$

$$[H_2^+](0) = I_0, \quad [H, H^+](0) = 0, \quad [H, H](0) = 0. \tag{C10}$$

The L_{ef} parameter is the effective thickness of the target gas layer that the secondary ions passes from the point of their formation to the Faraday cup. The exact solutions to the above equations are

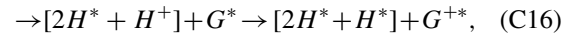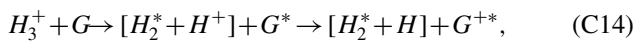$$[H_2^+](N) = I_0 e^{-(\sigma_d + \sigma_{10})LN}, \tag{C11}$$

$$[H, H^+](N) = I_0 \frac{\sigma_d L}{(\sigma_d + \sigma_{10})L - \sigma_2 L_{ef}}$$
$$\times [e^{-\sigma_2 L_{ef} N} - e^{-(\sigma_d + \sigma_{10})LN}], \tag{C12}$$

$$[H, H](N) = I_0 \frac{1}{(\sigma_d + \sigma_{10})L - \sigma_2 L_{ef}}\big[\sigma_d L(1 - e^{-\sigma_2 L_{ef} N})$$
$$+ (\sigma_{10}L - \sigma_2 L_{ef})(1 - e^{-(\sigma_d + \sigma_{10}LN)})\big]. \tag{C13}$$

In order to estimate the influence of secondary processes that affect the recorded ion current, Fig. 7 presents the solutions of the set of differential equations (B7)–(B9) calculated for the H_2^+ and H_3^+ ions with the CO molecule for different values of the present parameters. In calculations for the H_2^+ ions, the charge-exchange cross sections for the secondary H^+ disintegration products were assumed to be $\sigma_2 = 18$ Å^2, a value of the electron capture cross section determined in the present studies for $H^+ + CO$. In our studies we have found that the experimental attenuation plots are well approximated by a single-exponent function, represented on the plots by the circles. From the analysis of Fig. 7(a) we can see that assuming the unknown disintegration cross section σ_d to be about 1/4 of the observed charge-exchange cross section, to have the final ion current (expressed as the sum of $[H_2^+](N) + [H^+](N)$) close to the single exponent model, this will increase the σ_{10} only by 0.5 and 2 Å^2 for $L_{ef} = L/2$ and $L/8$, dashed and continuous line, respectively. By increasing the σ_d two times, we see that the deviation from the single exponential model is also rather small.

Figure 7(c) presents pressure dependency of the independent components (B11), (B12), and (B13) of the ion beam calculated for σ_d and L_{ef} parameters equal to 1/4 of the $\sigma_{10} = 14$ Å^2 and $L = 4.4$ cm. The black continuous line is the fractional concentration of the primary H_2^+ ions in the beam after passing the L path, the dash-dot-dot line is the fractional concentration of the disintegrated secondary ions (in other words an amount of [H,H$^+$] pairs), and the red dash-dot line is the fractional concentration of the neutral components in the beam ([H,H] present in the form of H$_2$ molecule or two independent hydrogen atoms) which are not registered in the Faraday cup. The blue dashed line is the resulting ion current as the sum of the [H$_2^+$] and [H,H$^+$] components.

For the H$_3^+$ ions, there are even more disintegration channels besides the charge-exchange process:

$$H_3^+ + G \rightarrow [H_2^* + H^+] + G^* \rightarrow [H_2^* + H] + G^{+*}, \quad (C14)$$

$$\rightarrow [H_2^{+*} + H^*] + G^* \rightarrow [H_2^+ + H^*] + G^{+*}, \quad (C15)$$

$$\rightarrow [2H^* + H^+] + G^* \rightarrow [2H^* + H^*] + G^{+*}, \quad (C16)$$

$$\rightarrow H_2^* + H^* + G^{*+} \quad (CE), \quad (C17)$$

where H$_3^+$ could disintegrate into fast H$^+$ or H$_2^+$ components, which undergo the attenuation with different rates and affect the recorded ion current

$$H_3^+ \xrightarrow{\sigma_d} \left(\begin{array}{c} [H_2, H^+] \\ [H_2^+, H] \end{array} \right) \xrightarrow{\sigma_2} [H_2, H], \quad (C18)$$

$$H_3^+ \xrightarrow{\sigma_{10}} [3H] \quad (CE), \quad (C19)$$

The solutions of the differential equations for the H$_3^+$ ions are presented in Fig. 7(b). Setting the σ_d equal to $\sigma_{10}/3$ or $3\sigma_{10}$ and $L_{ef} = L/8$ we see that in present conditions the resultant ion current is very close to the single exponential function for σ_{10} increased by 0.05 and 0.6 Å^2, respectively. Figure 7(d) presents pressure dependency of the independent components of the H$_3^+$ ion beam calculated for $\sigma_d = 1$ Å^2 and $L_{ef} = 0.55$ cm.

[1] D. H. Wooden, S. B. Charnley, and P. Ehrenfreund, in *Comets II*, edited by M. C. Festou, H. U. Keller, and H. A. Weaver (The University of Arizona Press, Tucson, AZ, 2004), p. 33.

[2] D. Despois, N. Biver, D. Bockelée-Morvan, and J. Crovisier, in *Proceedings IAU Symposium No. 231, Astrochemistry—Recent Successes and Current Challenges*, edited by D. C. Lis, G. A. Blake, and E. Herbst (IAU, Paris, 2005), p. 119.

[3] D. Bockelée-Morvan, J. Crovisier, M. J. Mumma, and H. A. Weaver, in Ref. [1], p. 391.

[4] M. E. Rudd, R. D. DuBois, L. H. Toburen, C. A. Ratcliffe, and T. V. Goffe, Phys. Rev. A **28**, 3244 (1983).

[5] M. E. Rudd, T. V. Goffe, A. Itoh and R. D. DuBois, Phys. Rev. A **32**, 829 (1985).

[6] M. Sataka, A. Yagishitat, and V. Nakai, J. Phys. B **23**, 1225 (1990).

[7] T. Kusakabe, K. Asahina, J. P. Gu, G. Hirsch, R. J. Buenker, M. Kimura, H. Tawara, and Y. Nakai, Phys. Rev. A **62**, 062714 (2000).

[8] B. G. Lindsay, W. S. Yu, and R. F. Stebbings, Phys. Rev. A **71**, 032705 (2005).

[9] J. B. Greenwood, A. Chutjian, and S. J. Smith, Astrophys. J. **529**, 605 (2000).

[10] T. Kusakabe, S. Kitamuro, Y. Nakai, H. Tawara, and M. Sasao, Plasma Fusion Res. **7**, 2401062 (2012).

[11] T. F. Moran and R. J. Conrads, J. Chem. Phys. **58**, 3793 (1973).

[12] M. Gruntman, J. Geophys. Res. A **101**, 15555 (1996).

[13] D. Smith, P. Spanel, and T. J. Millar, Mon. Not. R. Astron. Soc. **266**, 31 (1994).

[14] D. W. Koopman, Phys. Rev. **166**, 57 (1968).

[15] M. A. Coplan and K. W. Ogilvie, J. Chem. Phys. **52**, 4154 (1970).

[16] B. N. Wan and H. Langhoff, J. Chem. Phys. **97**, 8137 (1992).

[17] B. Pranszke, Chem. Phys. Lett. **508**, 197 (2011).

[18] B. Pranszke, Chem. Phys. Lett. **499**, 199 (2010).

[19] B. Pranszke, Chem. Phys. Lett. **536**, 26 (2012).

[20] S. Werbowy and B. Pranszke, Astrophys. J. **780**, 157 (2014).

[21] A. Ehbrecht, A. Kowalski, and Ch. Ottinger, Int. J. Mass Spectrom. Ion Processes **156**, 41 (1996).

[22] B. Pranszke, S. Werbowy, and A. Lawicki, Phys. Rev. A **83**, 032707 (2011).

[23] S. Werbowy and B. Pranszke, Astron. Astrophys. **535**, A51 (2011).

[24] A. Kowalski, B. Pranszke, S. Werbowy, and Ch. Ottinger, Chem. Phys. Lett. **389**, 218 (2004).

[25] A. Itoh and M. E. Rudd, Phys. Rev. A **35**, 1937 (1987).

[26] R. S. Gao, L. K. Johnson, C. L. Hakes, K. A. Smith, and R. F. Stebbings, Phys. Rev. A **41**, 5929 (1990).

[27] I. Čadež *et al.*, J. Phys. B **35**, 2515 (2002).

[28] M. A. Coplan and K. W. Ogilvie, J. Chem. Phys. **61**, 2010 (1974).

[29] A. Kramida, Yu. Ralchenko, J. Reader, and NIST ASD Team, NIST Atomic Spectra Database (ver. 5.3) [Online]. Available: http://physics.nist.gov/asd [2016, January 7]. National Institute of Standards and Technology, Gaithersburg, MD.

[30] S. G. Lias, Ionization Energy Evaluation in *NIST Chemistry WebBook*, NIST Standard Reference Database Number 69, edited by P. J. Linstrom and W. G. Mallard (National Institute of Standards and Technology, Gaithersburg, MD), http://webbook.nist.gov (retrieved January 7, 2016).

[31] S. G. Lias, R. D. Levin, and S. A. Kafafi, Ion Energetics Data in Ref. [30].

[32] B. deB. Darwent, Nat. Bur. Stand. (U.S.), Nat. Stand. Ref. Data Series **31**, 1 (1970).

[33] A. V. Mitin, Russ. J. Phys. Chem. A **84**, 2314 (2010).

[34] G. H. Bearman, J. D. Earl, R. J. Pieper, H. H. Harris, and J. J. Leventhal, Phys. Rev. A **13**, 1734 (1976).

[35] D. Strasser, J. Levin, H. B. Pedersen, O. Heber, A. Wolf, D. Schwalm, and D. Zajfman, Phys. Rev. A **65**, 010702(R) (2001).

[36] R. E. Olson, Phys. Rev. A **6**, 1822 (1972).

[37] M. Vujovic, M. Matic, B. Cobic, and Yu. S. Gordeevs, J. Phys. B **5**, 2085 (1972).

[38] S. Werbowy, A. Kowalski, and B. Pranszke, Chem. Phys. Lett. **641**, 136 (2015).

[39] R. Dagnac, D. Blanc, and D. Molina, J. Phys. B **3**, 1239 (1970).

[40] G. W. McClure, Phys. Rev. **130**, 1852 (1963).

[41] P. J. Chantry, J. Chem. Phys. **55**, 2746 (1971).

[42] H. M. Rosenstock, K. Draxl, B. W. Steiner, and J. T. Herron, in Ref. [31] (retrieved January 15, 2016).

[43] A. V. Turbiner and J. C. Lopez Vieyra, J. Phys. Chem. A **117**, 10119 (2013).

[44] C. T. Russell and O. Vaisberg, *Venus* (University of Arizona Press, Tucson, AZ, 1983).

[45] J. G. Luhmann and C. T. Russell, *Encyclopedia of Planetary Sciences* (Chapman and Hall, New York, 1997).